

AdvMIL: Adversarial Multiple Instance Learning for the Survival Analysis on Whole-Slide Images ^{*,**}

Pei Liu^a, Luping Ji^{a,*}, Feng Ye^b, Bo Fu^a

^aSchool of Computer Science and Engineering, University of Electronic Science and Technology of China, Xiyuan Ave, Chengdu, 611731, Sichuan, China

^bInstitute of Clinical Pathology, West China Hospital, Sichuan University, Guo Xue Xiang, Chengdu, 610041, Sichuan, China

Abstract

The survival analysis on histological whole-slide images (WSIs) is one of the most important means to estimate patient prognosis. Although many weakly-supervised deep learning models have been developed for gigapixel WSIs, their potential is generally restricted by classical survival analysis rules and fully-supervision requirements. As a result, these models provide patients only with a completely-certain point estimation of time-to-event, and they could only learn from the well-annotated WSI data currently at a small scale. To tackle these problems, we propose a novel adversarial multiple instance learning (AdvMIL) framework. This framework is based on adversarial time-to-event modeling, and it integrates the multiple instance learning (MIL) that is much necessary for WSI representation learning. It is a plug-and-play one, so that most existing WSI-based models with embedding-level MIL networks can be easily upgraded by applying this framework, gaining the improved ability of survival distribution estimation and semi-supervised learning. Our extensive experiments show that AdvMIL could not only bring performance improvement to mainstream WSI models at a relatively low computational cost, but also enable these models to learn from unlabeled data with semi-supervised learning. Our AdvMIL framework could promote the research of time-to-event modeling in computational pathology with its novel paradigm of adversarial MIL.

Keywords: Computational Pathology, Whole-Slide Image, Survival Analysis, Time-to-event Modeling, Multiple Instance Learning, Generative Adversarial Network

1. Introduction

Survival analysis, also known as time-to-event analysis, is one of the primary statistical approaches for analyzing data on time to event (Cox, 1975; Kalbfleisch and Prentice, 2011). It is usually adopted in medical fields to analyze clinical materials and assist doctors in understanding disease prognosis (Wulczyn et al., 2021). Histological whole-slide image (WSI) is one of these materials. It is produced by scanning tissue slides (millimeter scale) with a high-end microscope. Compared to the materials like demographics and genomics, digitized WSIs contain unique hierarchical structures at a gigapixel-resolution (Zarella et al., 2018), e.g., tissue phenotype, tumor microenvironment, and cellular morphology. These microscopic structures could provide very valuable cues for the prognosis of tumor diseases (Yu et al., 2016; Chen et al., 2022b), contributing to the improvement of patient management and disease outcomes (Nir et al., 2018; Kather et al., 2019; Skrede et al., 2020).

Unlike regular natural images, histological WSIs are usually with an extremely-high resolution, e.g., $40,000 \times 40,000$ pixels. This poses great challenges to WSI analysis and modeling,

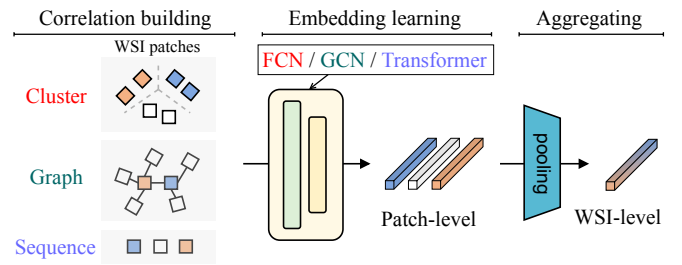


Figure 1: Paradigm of embedding-level multiple-instance learning for WSI representation learning. The structure of cluster, graph, or sequence is usually adopted to build patch correlations. These correlations are utilized by different networks to learn WSI-level representations.

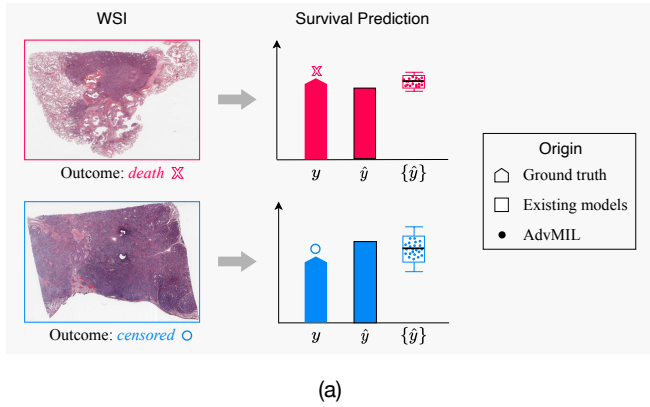
especially the global representation learning of WSIs. To tackle these challenges, many methods follow a weakly-supervised framework with three stages: (i) WSI patching, (ii) patch-level feature extracting, and (iii) slide-level representation learning (Chen et al., 2022a; Ghaffari Laleh et al., 2022). In procedure, these methods derive global representations through building patch correlations, learning patch-level embeddings, and aggregating these embeddings, as shown in Figure 1. This procedure is also cast as embedding-level multiple instance learning (MIL) (Ilse et al., 2018; Carbonneau et al., 2018). According to the type of patch correlation, the mainstream MIL-based methods of survival analysis can be roughly divided into three

*This work is under review.

**Source code is available at <https://github.com/liupei101/AdvMIL> for facilitating further research.

*Corresponding author: L. Ji (jiluping@uestc.edu.cn).

Email address: yuuki1p@163.com (Pei Liu)



(a)

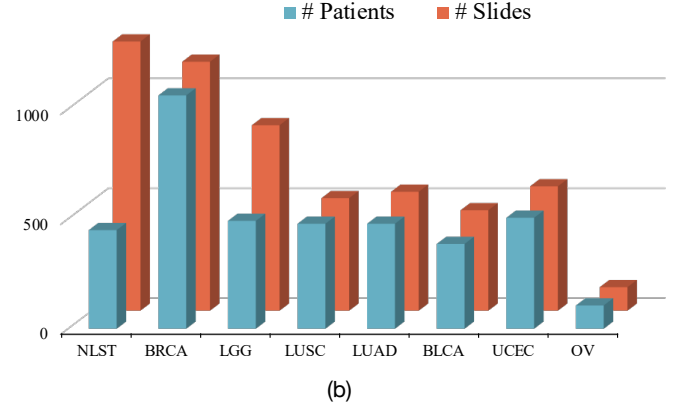


Figure 2: The commonality of existing WSI survival analysis methods in model output and input: (a) model output, existing methods are limited to a point time-to-event estimation, whereas ours can provide an estimation of time-to-event distribution, believed to be more robust and interpretable; (b) model input, all the most commonly-used datasets for WSI survival analysis are at a very small scale, usually with around 1,000 slides.

categories: cluster-based (Yao et al., 2020; Shao et al., 2021), graph-based (Li et al., 2018; Chen et al., 2021), and sequence-based (Huang et al., 2021; Shen et al., 2022; Liu et al., 2022).

Although there are many kinds of methods for the survival analysis of gigapixel WSIs, these methods are generally restricted by the classical survival analysis rules that include a certain survival assumption regarding hazard function (Cox, 1975; Kalbfleisch and Prentice, 2011; Liu et al., 2021) and a likelihood estimation of discrete time domain (Zadeh and Schmid, 2021). This leads to a point survival estimation of them. However, the output of point estimation, compared with that of distribution estimation illustrated in Figure 2(a), represents a single completely-certain result believed to be lacking in predictive robustness and interpretability (Lakshminarayanan et al., 2017; Kendall and Gal, 2017; Nazarovs et al., 2022; Linmans et al., 2023). In addition, from the perspective of input, all these methods train their own networks with slide-level labels, following a fully-supervised setting. This means that their networks need sufficient labeled data for training to make the models well-generalized to unseen samples. However, among current publicly-available WSI datasets, the number of qualified patients is limited to around 500 in most cases, as shown in Figure 2(b). By contrast, the standard datasets in deep learning, such as ImageNet (Deng et al., 2009), often contains more than 10,000 samples. This fact indicates that current WSI-based survival analysis is still in a small data regime that is believed to have adverse effects on the generalization ability of deep learning models (Chapelle et al., 2009; Zhou, 2021; Marini et al., 2021).

Generative adversarial network (GAN) (Goodfellow et al., 2014a) offers means to mitigate these problems. On one hand, GAN is a generative model capable of estimating complex data distribution via implicitly sampling, naturally fit for predictive distribution modeling. On the other hand, the generator-discriminator structure of GAN can take fake (or unlabeled) samples as input, just meeting the needs of semi-supervised learning (Goodfellow, 2016). In this way, GAN-based models are never limited to certain point estimation or fully-supervised settings; instead, they provide robust distribution outputs, and

notably, they learn from unlabeled data to enhance their generalization ability (Springenberg, 2015; Salimans et al., 2016; Miyato et al., 2018; Li et al., 2021).

In the past few years, GAN has attracted great attention and inspired many interesting applications beyond image generation (Gui et al., 2021). Survival analysis is one of them. It is first combined with a conditional GAN (cGAN) (Mirza and Osindero, 2014), referred to as adversarial time-to-event modeling, in order to develop a general assumption-free survival model for analyzing clinical tabular data (Chapfuwa et al., 2018, 2020). Afterward, this general model is successfully extended to convolutional neural networks for the time-to-event modeling of CT images (Uemura et al., 2021). These models have shown promising results, especially their advantages of predictive accuracy and robustness. Further adoption of GAN for survival analysis in computational pathology is strongly anticipated, since the current time-to-event modeling of WSIs still face the problems posed by its inherent classical modeling paradigm mentioned before.

In this study, we propose a novel framework for the survival analysis on gigapixel whole-slide images, referred to as adversarial multiple instance learning (AdvMIL). This framework no longer relies on the classical paradigm of time-to-event modeling; instead, it is based on adversarial time-to-event modeling and integrates the multiple instance learning that is much necessary for WSI representation learning. As a result, most existing embedding-level MIL networks can be easily integrated into the proposed AdvMIL framework, thereby gaining the ability of survival distribution estimation and semi-supervised learning without introducing extra techniques. The results on three publicly-available WSI datasets verify that AdvMIL could often bring performance improvements to mainstream MIL networks at a relatively low computational cost; and most importantly, it could enable current models to enhance their generalization ability by learning from unlabeled data in a semi-supervised manner.

The key contributions of our work are as follows:

- i) We present an adversarial multiple instance learning (AdvMIL) framework for the survival analysis on gigapixel whole-

slide images. Most existing WSI-based survival analysis models with embedding-level MIL networks can be upgraded by applying this framework, thereby gaining the ability of survival distribution estimation and semi-supervised learning. To our best knowledge, the proposed AdvMIL is the first work to adopt GANs in computational pathology for survival analysis.

ii) We demonstrate how a GAN can be combined with MIL paradigm to perform survival prediction on gigapixel WSIs, by the two key components of AdvMIL: the MIL encoder in generator and the fusion network with region-level instance projection (RLIP) in discriminator.

iii) We further explore how to train existing WSI models with our AdvMIL framework in a semi-supervised manner. Moreover, we propose a k -fold training strategy to make the semi-supervised learning more effective.

iv) We validate the effectiveness of AdvMIL through the extensive experiments on a total of 3,101 WSIs from three publicly-available datasets. Empirical results suggest that AdvMIL could boost the development of time-to-event modeling in computational pathology by introducing a novel adversarial MIL paradigm.

2. Related work

2.1. Survival analysis of WSIs

Predicting time-to-event from digitized gigapixel WSIs is an active field in these years. Here we review some representative works, focusing on their networks and survival loss functions.

(1) Multiple-instance learning network

To learn global representations from gigapixel WSIs, the paradigm of MIL (see Figure 1) is widely adopted in end-to-end deep learning models (Ghaffari Laleh et al., 2022). These models usually deploy different backbones for different patch correlations, *e.g.*, fully-connected networks for cluster, graph convolution networks (Kipf and Welling, 2016) for graph, and Attention-MIL (Ilse et al., 2018) or ViT (Dosovitskiy et al., 2020) for sequence. In procedure, these networks first transfer patch information along patch correlations to learn non-local patch-level embeddings, and then extract WSI representation by pooling these embeddings into a global vector.

(2) Survival loss function

Most models make assumptions on survival hazard function (Kalbfleisch and Prentice, 2011) for survival analysis. Cox proportional hazard (Cox, 1975) and accelerated failure time (Wei, 1992) are the two most classical assumptions. The loss functions based on these two assumptions are very popular in WSI survival modeling, owing to their simplicity and interpretability. In addition, the survival loss function based on a maximum likelihood estimation, which has demonstrated good calibration and discrimination on tabular data (Zadeh and Schmid, 2021), is adopted by Chen et al. (2021, 2022a); Liu et al. (2022) to analyze WSI data. It requires a pre-discretization of survival time although it's assumption-free. These loss functions are derived from a class of discriminative models, leading to the single point estimation of time-to-event.

2.2. Adversarial time-to-event analysis

(1) Generative adversarial network

GAN is a powerful generative model (Goodfellow et al., 2014a) that has a wide variety of vision applications (Gui et al., 2021), such as image generation, denoising, and editing. Additionally, it also has been extensively studied to perform semi-supervised learning (Springenberg, 2015; Carmon et al., 2019) or to enhance the robustness of deep learning networks (Goodfellow et al., 2014b; Miyato et al., 2018). Following GAN, a conditional GAN (cGAN) (Mirza and Osindero, 2014) is first proposed in order to improve the quality of generated images by incorporating conditional labels. Based on cGAN, many efforts have been made to better exploit the information of conditional labels. The projection discriminator (Miyato and Koyama, 2018), as a representative work of cGAN, is one of them. It projects a conditional vector on input's final embedding, originally developed for a general application on regular natural images.

(2) Time-to-event modeling via conditional GAN

It is seen in DATE (Chapfuwa et al., 2018) for the first time, motivated by the fact that cGAN can capture complex data distribution (Goodfellow et al., 2014a). Like cGAN, DATE also uses a generator-discriminator network. Specifically, the generator G estimates a conditional distribution of time-to-event

$$\hat{t} = G(x, \mathcal{N}) \sim P_{t|x},$$

where x denotes a conditional input and \mathcal{N} denotes a noise input. The discriminator D recognizes the real input (x, t) or the fake input (x, \hat{t}) , where t is the label of time-to-event associated with x . Such adversarial generative manner inherent in cGAN enables DATE to estimate the distribution of time-to-event via implicitly sampling from G , rather than via learning and optimizing the parameters of a priori distribution.

DATE is a general assumption-free model of time-to-event analysis, originally applied to clinical tabular data. Following the framework of DATE, pix2surv (Uemura et al., 2021) is further developed with convolutional networks for CT images. The researches of time-to-event modeling on tabular data and CT images have benefited from generative schemes, and have demonstrated better predictive accuracy and robustness. However, on computational pathology it still remains open. Moreover, how to perform semi-supervised learning, and whether the semi-supervised learning is effective to survival analysis tasks, are not yet studied in DATE and pix2surv.

In Section 3, we show how the framework of adversarial time-to-event modeling can be generalized to MIL paradigm to perform survival prediction tasks on gigapixel WSIs.

3. Methodology

We show our Adversarial Multiple Instance Learning (AdvMIL) framework in Figure 3. In a nutshell, AdvMIL generalizes adversarial time-to-event modeling to MIL paradigm by its two key components: the MIL encoder in generator and the fusion network with region-level instance projection (RLIP) in discriminator. At the end of this section, we describe how to

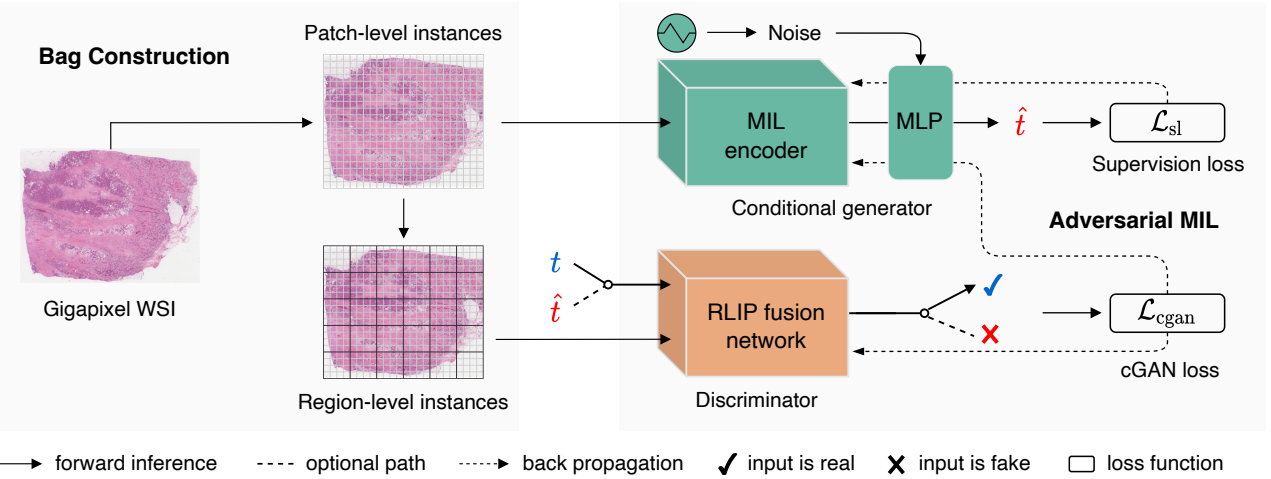


Figure 3: AdvMIL overview. A gigapixel WSI is transformed into a bag of patch-level instances. These instances are further grouped into regions. A general MIL network is adopted as the backbone of conditional generator. A RLIP (region-level instance projection) fusion network, elaborated in Figure 4, is proposed to implement discriminator. Conditional generator is optimized by both $\mathcal{L}_{\text{cGAN}}$ and \mathcal{L}_{sl} . Noise is represented by a high-dimensional vector with a certain distribution.

perform semi-supervised training with AdvMIL and a k -fold training strategy.

3.1. Preliminary

(1) Bag construction of WSIs

We roughly follow an easy-to-use recipe from CLAM (Lu et al., 2021) to prepare the bag construction of gigapixel WSIs. Specifically for each WSI, at first we fix its magnification at $f \times$ ($20 \times$ is a typical setting). Then we slice this image into a series of non-overlapping small patches of size $a \times a$ pixels, where those background patches are discarded. Finally, we apply an image feature extractor to all remaining patches, obtaining a bag of patch features. We denote the bag of patch features from one patient by

$$X \in \mathbb{R}^{m \times c} : \{x_j \in \mathbb{R}^c\}_{j=1}^m,$$

where m is the total number of patches in X , c is the dimensionality of patch features, and x_j denotes the j -th patch of X . m may be different across patients. Its common value is often more than 1,000 when $f = 20$.

(2) Notation convention

We denote survival data by $\mathcal{D} = \{(X_i, t_i, \delta_i)\}_{i=1}^{i=N}$, where X_i , t_i , and δ_i are the bag features, follow-up time, and censorship status of i -th patient, respectively. For the patients without censoring (i.e., with event occurrence), we denote their records by $\mathcal{D}_e = \{(X_i, t_i) | \delta_i = 0 \text{ for } i = 1, 2, \dots, N\}$. Similarly, the records of other patients with censoring are denoted as $\mathcal{D}_{ne} = \{(X_i, t_i) | \delta_i = 1 \text{ for } i = 1, 2, \dots, N\}$. For the i -th patient with $\delta_i = 1$, we only know that its real time-to-event is strictly later than t_i .

3.2. Adversarial multiple-instance learning

Next, we formulate our AdvMIL framework in the form of multiple instance learning.

(1) Generator

To make our framework not break away from MIL and cooperate smoothly with existing networks of WSI survival analysis,

we implement the generator with a general MIL encoder and a MLP (multi-layer perceptron) layer. This encoder is adopted to extract global bag representations. It could be any embedding-level MIL networks that output bag-level vectors, e.g., cluster-, graph-, or sequence-based ones. The MLP layer is utilized to process both bag-level vectors and noise inputs, producing time-to-event estimations.

For a given X (the bag from one patient), we denote its time-to-event estimation by

$$\hat{t} = G(X, \mathcal{N}), \quad \mathcal{N} \sim P_n = \mathbf{U}(0, 1),$$

where \mathcal{N} is a noise variable with uniform distribution, and G denotes the generator. In this way, G implicitly estimates the distribution of time-to-event via sampling from \mathcal{N} . This distribution output by G is expected to match the realistic conditional distribution of time-to-event on given X , i.e., $P_{t|X}$. By the noise-outsourcing lemma (Kallenberg, 2002) from probability theory under minimal conditions, the existence of G can be guaranteed (Zhou et al., 2022), namely,

$$\exists G, \text{s.t. } \hat{t} = G(X, \mathcal{N}) \sim P_{t|X}. \quad (1)$$

Since \mathcal{N} is an independent variable, Eq. (1) can be further written as its joint distribution form,

$$(X, G(X, \mathcal{N})) \sim P_{(X,t)}, \quad (2)$$

where G can be found by optimizing a cGAN (Mirza and Osindero, 2014) with X as its conditional input.

(2) Discriminator

The discriminator, denoted as D , aims to distinguish between the fake pair, (X, \hat{t}) sampled from G , and the real pair, (X, t) sampled from realistic data distribution. However, existing discriminators cannot be directly adopted to achieve this purpose, since D is required to efficiently process the fusion of the X associated with an extremely-large matrix and the t associated

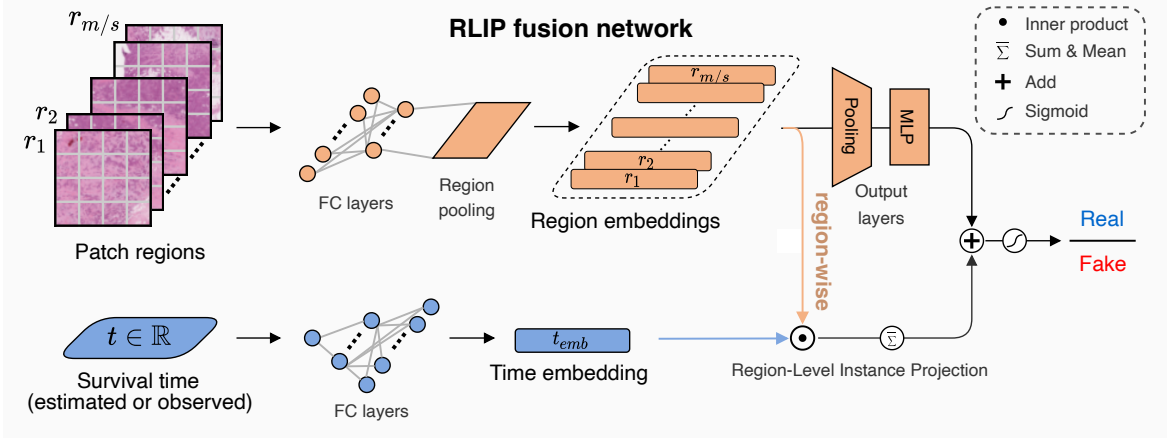


Figure 4: Fusion Network with Region-Level Instance Projection (RLIP). It comprises two key parts: a WSI region embedding and a region-level instance projection, where $r_1, r_2, \dots, r_{m/s}$, denote a series of region identifiers regions. FC and MLP indicate a fully-connected network and a multi-layer perceptron, respectively.

with one single real value. To tackle this challenge, we propose a novel fusion network with region-level instance projection (RLIP), as shown in Figure 4. It can deal with the fusion of big matrix and scalar value, inspired by projection discriminator (Miyato and Koyama, 2018). Moreover, our implementation of D would not bring too much computational overheads to existing mainstream MIL models, as shown in Section 4.2.

Specifically, we assume that there is a region partition so that (i) all the m patches of X are divided into several disjoint subsets and (ii) each subset presents a connected region of WSI. An alternative and straightforward solution is to slice each WSI into bigger image patches of size $\eta a \times \eta a$ pixels at first, and then to further slice each patch into η^2 (denoted as $s = \eta^2$) small pixel patches of size $a \times a$ pixels. As a result, we obtain $\frac{m}{s}$ patch subsets, denoted as $r_1, r_2, \dots, r_{m/s}$. Note that the scheme of region partition could be flexible enough since our discriminator is devised to be capable of working under various settings of patch regions (even if these regions have different sizes). Please see the implementation of D in Section 4.1.

After region partition, those patches are transformed into region-level embeddings, $X_{emb} : \{v_\tau \in \mathbb{R}^{c'}\}_{\tau=r_1}^{r_{m/s}}$, by a region embedding layer ϕ . Then, X_{emb} is mapped into a scalar output indicating the likelihood of real pairs, by a global attention pooling layer (denoted as gap) and a binary prediction head ψ . The scalar time, denoted as t , is embedded as a vector with c' dimensions by a MLP φ . X_{emb} and t_{emb} are fused through a *region-wise* inner product. We write the final output of D by

$$y_D = \psi(gap(X_{emb})) + \frac{1}{m/s} \sum_{v_\tau \in X_{emb}} v_\tau \cdot t_{emb}. \quad (3)$$

(3) Network training

As shown in Figure 3, we use the two loss functions, cGAN loss and supervision loss, to optimize our network. cGAN loss is a general adversarial loss (Goodfellow et al., 2014a) that involves D and G , written as

$$\begin{aligned} \mathcal{L}_{cgan} = \min_G \max_D & \mathbb{E}_{(X, t) \sim P_{\mathcal{D}_e}} \log D(X, t) \\ & + \mathbb{E}_{X \sim P_X, N \sim P_n} \log [1 - D(X, G(X, N))], \end{aligned} \quad (4)$$

where D is optimized to accurately recognize real or fake pairs while G fools D by generating the time-to-event that is expected to better match realistic data distribution. Note that (X, t) is drawn from $P_{\mathcal{D}_e}$, instead of $P_{\mathcal{D}}$, in the first term of Eq. (4), because only the patients with event occurrence have the ground truth label of time-to-event.

Like most cGANs, the convergence of \mathcal{L}_{cgan} is guaranteed theoretically (Zhou et al., 2022). Nevertheless, during network training we observe that the adversarial network is very difficult to be optimized only by \mathcal{L}_{cgan} . This issue is open in adversarial learning (Goodfellow, 2016; Gui et al., 2021). To alleviate this problem, we additionally use an auxiliary supervision loss that fully utilizes time-to-event labels (Chapfuwa et al., 2018; Uemura et al., 2021), so as to better train the network and speed up its convergence. This auxiliary loss is written as

$$\begin{aligned} \mathcal{L}_{sl} = \min_G & \mathbb{E}_{(X, t) \sim P_{\mathcal{D}_e}, N \sim P_n} |G(X, N) - t| \\ & + \mathbb{E}_{(X, t) \sim P_{\mathcal{D}_{ne}}, N \sim P_n} \text{ReLU}(t - G(X, N)), \end{aligned} \quad (5)$$

and is leveraged to optimize G . As shown in Eq. (5), \mathcal{L}_{sl} takes both censored and uncensored patients into account. This thus enables G to narrow its empirical errors on both $P_{\mathcal{D}_e}$ and $P_{\mathcal{D}_{ne}}$. Unlike other loss functions that are widely adopted in WSI survival analysis, \mathcal{L}_{sl} no longer relies on any hazard function assumption or time pre-discretization, so AdvMIL can estimate time-to-event distribution via implicit sampling.

The procedure of training AdvMIL is similar to that of training vanilla GAN. Specifically, it can be also viewed as an adversarial min-max game between G and D . The key difference between AdvMIL and vanilla GAN lies in that training AdvMIL would involve censored patients (\mathcal{D}_{ne}) and supervision loss (\mathcal{L}_{sl}). We show the details of training AdvMIL in Alg. 1.

3.3. *k*-fold semi-supervised learning

Here we describe how to perform semi-supervised training with AdvMIL for survival analysis tasks. Furthermore, we introduce a *k*-fold training strategy to make the semi-supervised learning more effective.

Algorithm 1: Mini-batch training with AdvMIL (one epoch).

```

Input: generator  $G$ , discriminator  $D$ , noise  $\mathcal{N}$ , batch size  $b$ , cGAN loss  $\mathcal{L}_{\text{cgan}}$ , supervision loss  $\mathcal{L}_{\text{sl}}$ , and training data  $\mathcal{D}_{\text{train}} = \{(X_i, t_i, \delta_i)\}_{i=1}^{i=N}$ .
1 load mini-batch samples,  $B \leftarrow \{(X_i, t_i, \delta_i)\}_{i=1}^{i=b}$ 
// fix  $G$ , update  $D$ 
2  $\mathcal{R} \leftarrow \{\}$ 
3 foreach  $(X_i, t_i, \delta_i)$  in  $B$  do
4   if  $\delta_i = 0$  then
5      $\hat{y}_{\text{real}} \leftarrow D(X_i, t_i)$  // real pairs
6     append  $\hat{y}_{\text{real}}$  to  $\mathcal{R}$ 
7   end
8    $\hat{y}_{\text{fake}} \leftarrow D(X_i, G(X_i, \mathcal{N}))$ 
9   append  $\hat{y}_{\text{fake}}$  to  $\mathcal{R}$  // fake pairs
10 end
11 update  $D$  by optimizing the  $\mathcal{L}_{\text{cgan}}$  on  $\mathcal{R}$ 
// fix  $D$ , update  $G$ 
12  $\mathcal{R} \leftarrow \{\}, \mathcal{R}_{\text{sl}} \leftarrow \{\}$ 
13 foreach  $(X_i, t_i, \delta_i)$  in  $B$  do
14    $\hat{t}_i \leftarrow G(X_i, \mathcal{N})$ 
15   append  $(\hat{t}_i, t_i)$  to  $\mathcal{R}_{\text{sl}}$ 
16    $\hat{y}_{\text{fake}} \leftarrow D(X_i, \hat{t}_i)$  // fake pairs
17   append  $\hat{y}_{\text{fake}}$  to  $\mathcal{R}$ 
18 end
19 update  $G$  by optimizing the  $\mathcal{L}_{\text{cgan}}$  on  $\mathcal{R}$  and the  $\mathcal{L}_{\text{sl}}$  on  $\mathcal{R}_{\text{sl}}$ 

```

We denote training and test data by $\mathcal{D}_{\text{train}}$ and $\mathcal{D}_{\text{test}}$, respectively. To satisfy the setting of semi-supervised training, we assume that $\mathcal{D}_{\text{train}}$ is split into the two parts: labeled data (denoted as \mathcal{D}_{l}) and unlabeled data (denoted as \mathcal{D}_{ul}). In network training, all the samples from $\mathcal{D}_{\text{train}}$ will be fed into AdvMIL; the samples from \mathcal{D}_{ul} always keep label-invisible, *i.e.*, their labels would never be used.

In the absence of labels, \mathcal{D}_{ul} will only be used in the second term of Eq. (4). Namely, unlabeled samples are utilized to inference time-to-event estimations through G at first, and then are combined with these estimations as fake pairs to calculate $\mathcal{L}_{\text{cgan}}$ and optimize the networks associated with $\mathcal{L}_{\text{cgan}}$. Considering an extreme case that all the samples from $\mathcal{D}_{\text{train}}$ are label-invisible, the network would become hard to train, because fake pairs are dominant in network optimization. To alleviate this possible issue, we propose a k -fold semi-supervised training strategy. This strategy splits \mathcal{D}_{ul} into k folds and only one certain fold is reserved for one epoch training. Specifically, at T -th epoch, the $\mathcal{D}_{\text{train}}$ comprises \mathcal{D}_{l} and the α -th fold of \mathcal{D}_{ul} , where $\alpha = (T \bmod k)$. We show the details of k -fold semi-supervised training in Alg. 2.

4. Experiments and Results

4.1. Experimental settings

(1) Dataset description

There are three publicly-available WSI datasets used in this study. They are National Lung Screening Trial (NLST) (Team,

Algorithm 2: k -fold semi-supervised training with AdvMIL.

```

Input: training data  $\mathcal{D}_{\text{train}} = \{(X_i, t_i, \delta_i)\}_{i=1}^{i=N}$ , the number of training epochs  $\mathbb{T}$ , the number of folds  $k$ .
1  $\mathcal{D}_{\text{l}} \leftarrow \{(X_i, t_i, \delta_i) \mid t_i \text{ and } \delta_i \text{ is available}\}$  // labeled samples
2  $\mathcal{D}_{\text{ul}} \leftarrow \mathcal{D}_{\text{train}} \setminus \mathcal{D}_{\text{l}}$  // unlabeled samples
3 randomly split  $\mathcal{D}_{\text{ul}}$  into  $k$  folds:  $\mathcal{D}_{\text{ul}}^0, \mathcal{D}_{\text{ul}}^1, \dots, \mathcal{D}_{\text{ul}}^{k-1}$ 
4 for  $T \leftarrow 0$  to  $\mathbb{T} - 1$  do
5    $\mathcal{D}_{\text{train}} \leftarrow \mathcal{D}_{\text{l}}$ 
6   mini-batch training using Alg. 1
7    $\mathcal{D}_{\text{train}} \leftarrow \mathcal{D}_{\text{ul}}^{T \bmod k}$ 
8   mini-batch training using Alg. 1 // all the steps with  $t_i$  or  $\delta_i$  will be skipped
9 end

```

2011), BReast CAncer (BRCA), and Low-Grade Glioma (LGG), where both BRCA and LGG are from The Cancer Genome Atlas (TCGA) (Kandoth et al., 2013). Their examples are shown in Figure 5. Our criterion of dataset selection is mainly based on (i) the number of available patients, (ii) having been adopted in previous literature, and (iii) image quality. We finally collect a total of 3,101 WSIs from 1,911 patients without any subjective data curation. The overall survival of each dataset group is shown in Figure 6. The details of all datasets are presented in Table 1.

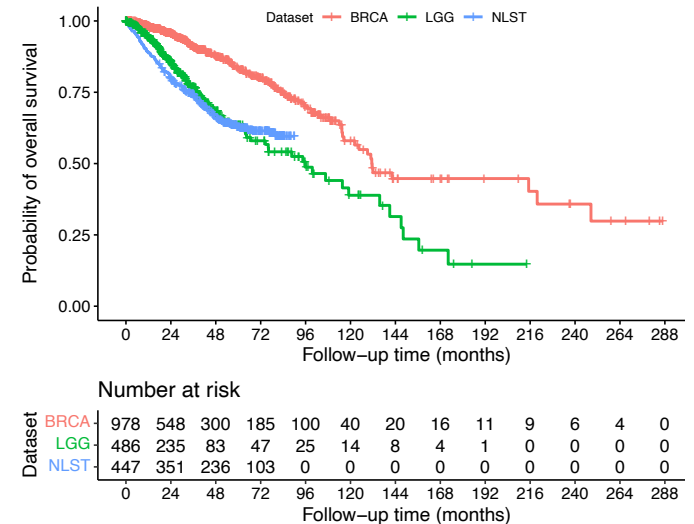


Figure 6: Survival curve of the patients in three datasets. Breast cancer patients have a better overall survival and longer follow-up time.

(2) Chosen Baselines

As shown in Table 2, the three methods, DeepAttnMISL (Yao et al., 2020), PatchGCN (Chen et al., 2021), and ESAT (Shen et al., 2022), are selected as our baselines, because (i) they belong to the three mainstream categories in end-to-end WSI modeling, *i.e.*, cluster-, graph-, and sequence-based, respectively; and (ii) they are the most representative ones in the

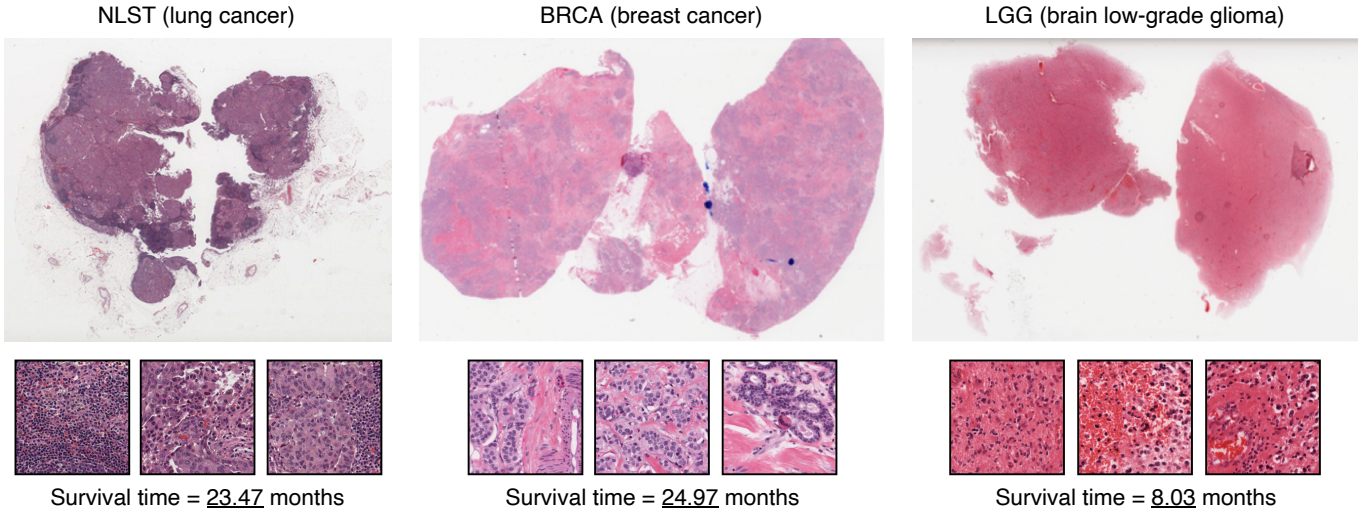


Figure 5: WSI samples and their representative patches from three primary sites. Most of these presented patches contain cancerous cells. There are much differences in cellular morphology between the tissues with different primary sites.

Table 1: Dataset details.

Item	NLST	BRCA	LGG
death ratio	35.9%	13.5%	23.4%
# patients	447	978	486
# WSIs	1,222	1,043	836
# patches	3,955,344	3,228,480	2,637,456
# patches / WSI	3,236.8	3,095.4	3,154.9

methods with the same category. Since AdvMIL can be applied to existing embedding-level MIL networks, we compare each baseline with the AdvMIL network in which the general MIL encoder is directly implemented by the MIL backbone of this baseline. Note that for fair comparisons the regression prediction head and the loss function of baselines are identical to that of AdvMIL networks. More details can be found in our publicly-available source code.

Table 2: Details of the baselines chosen for experiments.

Baseline	Category	Explanation
DeepAttnMISL (Yao et al., 2020)	Cluster	
PatchGCN (Chen et al., 2021)	Graph	
ESAT (Shen et al., 2022)	Sequence	Representative work of this category

(3) Implementation details

Bag construction. We set the magnification of WSIs to $20\times$ ($f = 20$), and the size of image patches to 256 ($a = 256$), because these are common choices that well balance computation efficiency and microscopic details. In addition, following CLAM (Lu et al., 2021), the feature extractor applied to image patches is an official truncated ResNet-50 model (He et al., 2016) that has been pre-trained on ImageNet (Deng et al., 2009), and $c = 1024$.

Generator. We empirically set the output dimension of MIL

Table 3: Full training settings.

Training parameter	Value
epoch	300
batch size	1
gradient accumulation step	16
early-stopping patience	30
early-stopping warm-up	5
learning rate for G	0.00008
learning rate for D	0.00008
optimizer	adam
weight decay rate	0.0005

encoder to 384 for both the patch-based model and the cluster-based model, and to 128 for the graph-based model (since it is efficient for training dense and large graphs). The MLP at the end of G has two layers, and at each layer N has the same dimension as input if N is added into this layer.

Discriminator. In the fusion network D , we use a fully-connected layer and an average pooling layer to implement the region embedding layer ϕ . Both these two layers are permutation-invariant so that they can work well with any number of patches, which indicates that the scheme of region partition can be flexible enough. The number of patches in each big region is set to 16 ($s = 16$). In our alternative scheme of region partition, the dimension of X_{emb} and t_{emb} are 128. ϕ is implemented by the MLP with two layers. The binary prediction head, ψ , consists of a fully-connected layer and a sigmoid function.

Network training. For model training, we update G by a simplified version of the second term of \mathcal{L}_{cgan} , *i.e.*,

$$\mathcal{L}_{cgan}(G) = \max_G \mathbb{E}_{X \sim P_X, N \sim P_N} D(X, G(X, N)),$$

to better train our adversarial network (Salimans et al., 2016). Full training settings are shown in Table 3. The learning rate of

Table 4: Performance of the model combining AdvMIL and patch-based ESAT. Other mainstream MIL networks are also examined and shown in Figure 7. The binary code in bracket is the setting of \mathcal{N} . Δ denotes the improvement brought by applying AdvMIL.

Patch-based	C-Index \uparrow			MAE \downarrow		
	NLST	BRCA	LGG	NLST	BRCA	LGG
ESAT (Shen et al., 2022)	0.653 _{0.047}	0.542 _{0.063}	0.638 _{0.091}	0.1920 _{0.0261}	0.0344 _{0.0056}	0.0518 _{0.0060}
ESAT + AdvMIL (0-1)	0.672 _{0.048}	0.545 _{0.065}	0.621 _{0.063}	0.1871 _{0.0203}	0.0383 _{0.0081}	0.0526 _{0.0058}
ESAT + AdvMIL (1-0)	0.649 _{0.039}	0.562 _{0.067}	0.642 _{0.076}	0.1995 _{0.0240}	0.0349 _{0.0065}	0.0522 _{0.0049}
ESAT + AdvMIL (1-1)	0.660 _{0.042}	0.545 _{0.075}	0.634 _{0.086}	0.1849 _{0.0153}	0.0366 _{0.0065}	0.0523 _{0.0051}
Δ	+ 2.91%	+ 3.69%	+ 0.63%	- 3.70%	+ 1.45%	+ 0.77%

G decays by a factor of 0.5 if validation loss doesn't decrease within 10 epochs. All hyper-parameters are identical for the three used datasets. Please see more details in our publicly-available source code.

(4) Evaluation metrics

We report the metrics most-commonly-used in survival analysis (Harrell Jr. et al., 1984), Concordance Index (C-Index), which measures the model ability of risk discrimination or ranking, just like the AUC in classification evaluation. We also record the Mean Absolute Error (MAE) of \hat{t} to ground truth, as calculated by Eq. (5). During evaluation, for one patient we get its \hat{t} by randomly sampling \mathcal{N} for only 30 times (as it's relatively time-consuming to do once inference for gigapixel WSIs). Given the limited times, we then use the median of \hat{t} as the final estimation for performance evaluation, because it is often more robust to outliers than a mean.

We use 5-fold Cross-Validation (CV) to evaluate each model. The 20% training set of each fold is used as a validation set for early stopping and model selection. Our data splitting is conducted at patient-level. All experiments run on a workstation with 2 \times NVIDIA V100s GPU.

4.2. Results and analysis

(1) Overall performance

The patch-based ESAT with AdvMIL. We first examine the effectiveness of applying AdvMIL to the patch-based ESAT. Compared to original ESAT, the model combining ESAT and AdvMIL is additionally optimized by $\mathcal{L}_{\text{cgan}}$ in adversarial learning. As we use the MLP with two layers at the end of G , there are three available noise settings, 0-1, 1-0, and 1-1, to determine if adding \mathcal{N} into MLP layers.

As shown in Table 4, we can see that (1) the model combining ESAT and AdvMIL outperforms its counterpart only with ESAT, by a C-Index improvement of 2.91%, 3.69% and 0.63% on NLST, BRCA and LGG, respectively; (2) Adding AdvMIL decreases the MAE on NLST by 3.70%, and the MAEs on the other two datasets just slightly increase by around +1%. These results suggest that the proposed AdvMIL framework has competitive advantages, especially on C-Index, for the patch-based model. Intuitively, by adversarial learning $\mathcal{L}_{\text{cgan}}$ could help to optimize G , and then make G become more robust to the input space extended and smoothed by \mathcal{N} (Miyato et al., 2018). In addition, from Table 4 we can find that \mathcal{N} 's setting also affects model performance. It indicates that a careful noise setting (the

focus of adversarial training (Goodfellow et al., 2014b)) could be a disturbance factor to AdvMIL's performance. More discussion of this can be seen in Section 4.3.

The cluster-based DeepAttnMISL and graph-based PatchGCN with AdvMIL. We test the adaptability of AdvMIL to other mainstream MIL networks (with distinct backbones). The experimental results are shown in Figure 7.

From these results, we can see that (1) the DeepAttnMISL model with AdvMIL can match or surpass its counterpart without AdvMIL at 4 out of 6 cases; (2) After applying AdvMIL to PatchGCN, the model performances are almost always superior to before, except the C-Index on LGG. These results show that AdvMIL could often well adapt to mainstream MIL networks, even if these networks have distinct backbones. Comparing the results of two baselines, we also notice that the cluster-based baseline often performs worse than the graph-based one.

It's worth noting that MAE is more sensitive to the value of \hat{t} than C-Index since C-Index measures the quality of estimation ranking—it only considers relative errors in measurement. Given the fact that limited estimations are drawn from G for evaluation, the final estimation of \hat{t} may be more likely to stray from the expectation of distribution, *i.e.*, $\mathbb{E}_{\mathcal{N} \sim P_n} P(t|X, \mathcal{N})$, resulting in worse MAEs, as shown in Table 4 and Figure 7.

(2) Computational overhead analysis

We evaluate the computation efficiency of discriminator in model size and inference cost, to verify if building D upon existing MIL networks will bring significant changes in computational overhead. Specifically, we measure the number of trainable parameters (# Params) for all used models. Moreover, to assess the theoretical amount of Multiply–Accumulate Operations (# MACs) in models, we randomly select a patient from NLST to do once model inference. This patient has a total of 3,360 patches in its WSI bag. The values shown in Table 5 are calculated by a Python toolkit, *ptflops*.

As shown in Table 5, D has 206.34K trainable parameters and 452.08M MACs. These numbers are obviously smaller than that of three generators. This suggests that it is reasonable for us to introduce such D to existing mainstream MIL networks, in view of computational overhead.

(3) k -fold semi-supervised training

We further investigate the potential of adopting AdvMIL in semi-supervised learning. This is not studied in both of the two classical works of adversarial survival analysis, *i.e.*, DATE (Chapfuwa et al., 2018) and pix2surv (Uemura et al., 2021). To

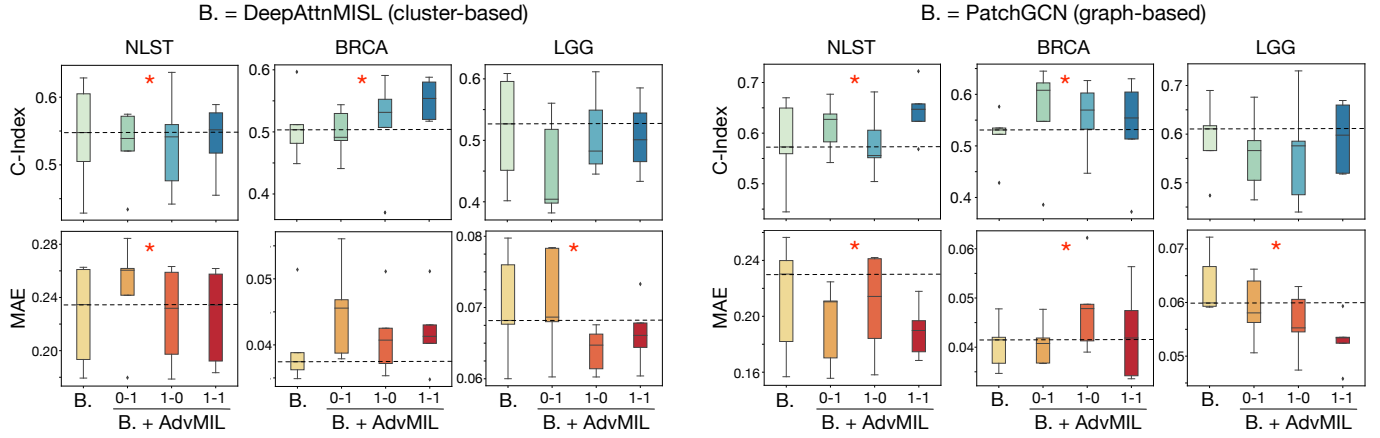


Figure 7: Adaptability of our AdvMIL to other mainstream MIL networks. Box-plots are from 5-fold CV. Horizontally-dotted line indicates a mean performance of given baseline. Asterisk (*) indicates that there is an improvement over baseline after applying our AdvMIL.

Table 5: The efficiency of network computation in parameters and MACs.

Network	# Params	# MACs
<i>D</i>	206.34K	452.08M
<i>G</i>	985.54K	1.33G
	PatchGCN	280.51K
	ESAT	1.73M

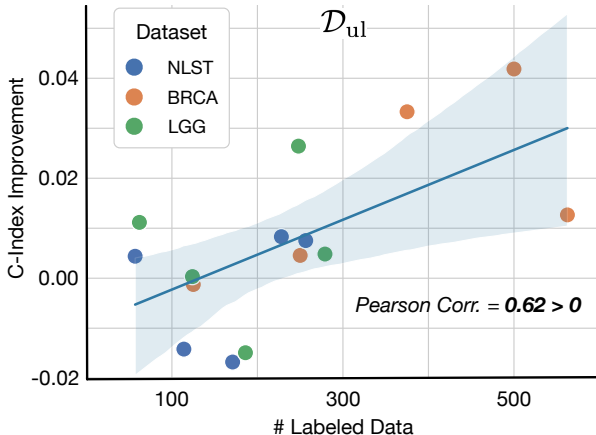


Figure 8: Performance improvement of k -fold semi-supervised training on \mathcal{D}_{ul} . Vertical axis gives the C-Index improvement of k -fold semi-supervised training over supervised training. The linear regression curve of all points is plotted, as well as a 95% confidence region, where ‘‘Corr.’’ represents ‘‘Correlation’’.

conduct this experiment, we set the ratio of \mathcal{D}_l , *i.e.*, $\mathcal{D}_l/\mathcal{D}_{train}$, to 0.2, 0.4, 0.6, 0.8, and 0.9 for each dataset. On one hand, we train AdvMIL only with \mathcal{D}_l , and take it as baseline for comparisons. On the other hand, we feed both \mathcal{D}_l and \mathcal{D}_{ul} into AdvMIL for k -fold semi-supervised training. The other settings keep the same. The patch-based ESAT is adopted, because it achieves the best overall performance among three MIL networks.

We firstly calculate the improvement of k -fold semi-supervised training over its baseline on \mathcal{D}_{ul} and \mathcal{D}_{test} , respectively. Then we visualize this improvement on a vertical axis of 2D plane, along with the size of \mathcal{D}_l on a horizontal axis. A

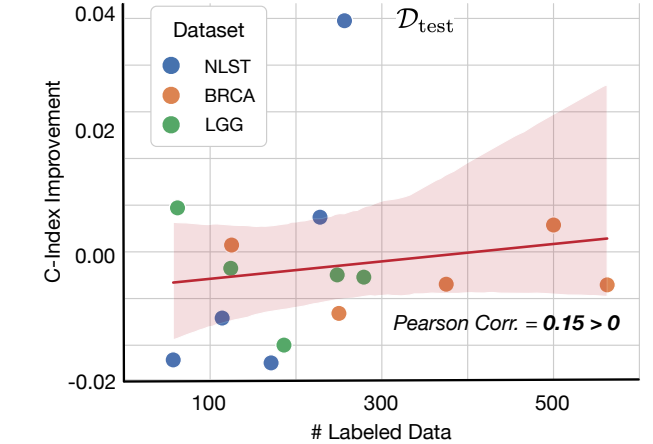


Figure 9: The performance improvement illustration of k -fold Semi-supervised Training on \mathcal{D}_{test} .

total of 15 points are obtained. The results on \mathcal{D}_{ul} and \mathcal{D}_{test} are shown in Figure 8 and Figure 9, respectively. Full numerical results can be seen in Table 6.

From these results, we can see that (1) on \mathcal{D}_{ul} , the improvements of C-Index are often positive (10 out of 15 points) and they would tend to be greater with the size of \mathcal{D}_l increasing (Pearson Corr. = 0.62); (2) on \mathcal{D}_{test} , the improvements of C-Index are positive in a few cases (5 out of 15 points), meanwhile they have a weakly-positive correlation with the size of \mathcal{D}_l (Pearson Corr. = 0.15). These findings mean that AdvMIL could be effective for predicting the label-invisible data *used* in training, while often losing its effectiveness for those label-invisible data *unused* in training. Namely, AdvMIL could be utilized to train with unlabeled WSIs so as to make the model well-generalized to unseen data and improve its own generation ability; whereas previous studies of survival analysis have not paid enough attention on this. Moreover, increasing the size of labeled training data would help to enlarge the C-Index improvement on \mathcal{D}_{ul} .

There are many studies that demonstrate GAN to be a promising and effective means for semi-supervised learning

Table 6: The k -fold semi-supervised training on AdvMIL. $\mathcal{D}_{\text{train}}$ is divided into label data (\mathcal{D}_{l}) and unlabeled data (\mathcal{D}_{ul}). We train AdvMIL on $\mathcal{D}_{\text{train}}$ and then measure its C-Index performances on both \mathcal{D}_{ul} and $\mathcal{D}_{\text{test}}$.

$\mathcal{D}_{\text{l}}/\mathcal{D}_{\text{train}}$	$\mathcal{D}_{\text{train}}$	\mathcal{D}_{ul} (C-Index)			$\mathcal{D}_{\text{test}}$ (C-Index)		
		NLST	BRCA	LGG	NLST	BRCA	LGG
0.2	\mathcal{D}_{l}	0.616 _{0.047}	0.553 _{0.029}	0.619 _{0.034}	0.623 _{0.082}	0.530 _{0.062}	0.602 _{0.055}
	$\mathcal{D}_{\text{l}} + \mathcal{D}_{\text{ul}}$ ($k=1$)	0.578 _{0.053}	0.545 _{0.043}	0.622 _{0.022}	0.576 _{0.055}	0.540 _{0.093}	0.608 _{0.041}
	$\mathcal{D}_{\text{l}} + \mathcal{D}_{\text{ul}}$ ($k=3$)	0.597 _{0.049}	0.542 _{0.047}	0.621 _{0.031}	0.616 _{0.077}	0.518 _{0.097}	0.592 _{0.059}
	$\mathcal{D}_{\text{l}} + \mathcal{D}_{\text{ul}}$ ($k=5$)	0.620 _{0.047}	0.552 _{0.049}	0.630 _{0.019}	0.610 _{0.065}	0.528 _{0.080}	0.610 _{0.048}
0.4	\mathcal{D}_{l}	0.632 _{0.047}	0.574 _{0.042}	0.603 _{0.053}	0.622 _{0.060}	0.579 _{0.135}	0.597 _{0.066}
	$\mathcal{D}_{\text{l}} + \mathcal{D}_{\text{ul}}$ ($k=1$)	0.602 _{0.027}	0.524 _{0.052}	0.595 _{0.090}	0.585 _{0.065}	0.527 _{0.085}	0.580 _{0.099}
	$\mathcal{D}_{\text{l}} + \mathcal{D}_{\text{ul}}$ ($k=3$)	0.618 _{0.051}	0.549 _{0.080}	0.604 _{0.062}	0.603 _{0.054}	0.536 _{0.069}	0.597 _{0.076}
	$\mathcal{D}_{\text{l}} + \mathcal{D}_{\text{ul}}$ ($k=5$)	0.606 _{0.050}	0.578 _{0.046}	0.592 _{0.085}	0.586 _{0.077}	0.576 _{0.037}	0.595 _{0.079}
0.6	\mathcal{D}_{l}	0.637 _{0.054}	0.532 _{0.058}	0.623 _{0.046}	0.646 _{0.043}	0.565 _{0.097}	0.649 _{0.045}
	$\mathcal{D}_{\text{l}} + \mathcal{D}_{\text{ul}}$ ($k=1$)	0.612 _{0.032}	0.556 _{0.030}	0.606 _{0.027}	0.610 _{0.083}	0.563 _{0.092}	0.639 _{0.045}
	$\mathcal{D}_{\text{l}} + \mathcal{D}_{\text{ul}}$ ($k=3$)	0.618 _{0.059}	0.535 _{0.060}	0.601 _{0.055}	0.645 _{0.040}	0.533 _{0.063}	0.637 _{0.063}
	$\mathcal{D}_{\text{l}} + \mathcal{D}_{\text{ul}}$ ($k=5$)	0.620 _{0.057}	0.566 _{0.060}	0.608 _{0.031}	0.632 _{0.059}	0.569 _{0.097}	0.625 _{0.046}
0.8	\mathcal{D}_{l}	0.629 _{0.044}	0.517 _{0.062}	0.609 _{0.048}	0.628 _{0.062}	0.538 _{0.089}	0.630 _{0.082}
	$\mathcal{D}_{\text{l}} + \mathcal{D}_{\text{ul}}$ ($k=1$)	0.638 _{0.049}	0.524 _{0.065}	0.590 _{0.039}	0.643 _{0.048}	0.552 _{0.072}	0.614 _{0.080}
	$\mathcal{D}_{\text{l}} + \mathcal{D}_{\text{ul}}$ ($k=3$)	0.623 _{0.075}	0.511 _{0.086}	0.635 _{0.092}	0.642 _{0.048}	0.567 _{0.093}	0.630 _{0.085}
	$\mathcal{D}_{\text{l}} + \mathcal{D}_{\text{ul}}$ ($k=5$)	0.622 _{0.032}	0.559 _{0.069}	0.615 _{0.038}	0.646 _{0.046}	0.554 _{0.085}	0.634 _{0.093}
0.9	\mathcal{D}_{l}	0.713 _{0.047}	0.470 _{0.139}	0.552 _{0.134}	0.661 _{0.038}	0.556 _{0.055}	0.637 _{0.085}
	$\mathcal{D}_{\text{l}} + \mathcal{D}_{\text{ul}}$ ($k=1$)	0.716 _{0.037}	0.482 _{0.187}	0.550 _{0.115}	0.650 _{0.062}	0.559 _{0.070}	0.641 _{0.066}
	$\mathcal{D}_{\text{l}} + \mathcal{D}_{\text{ul}}$ ($k=3$)	0.720 _{0.069}	0.449 _{0.202}	0.557 _{0.117}	0.654 _{0.055}	0.555 _{0.095}	0.619 _{0.050}
	$\mathcal{D}_{\text{l}} + \mathcal{D}_{\text{ul}}$ ($k=5$)	0.699 _{0.048}	0.380 _{0.154}	0.545 _{0.104}	0.664 _{0.051}	0.521 _{0.074}	0.637 _{0.060}

(Springenberg, 2015; Salimans et al., 2016; Miyato et al., 2018; Li et al., 2021; Gui et al., 2021). Our experiments also verify this, even in small data regimes ($\approx 1,000$ in our setting). In addition, we empirically find that our k -fold strategy ($k > 1$) could often lead to better results than the regular strategy without fold splitting, as shown in Table 6.

4.3. Ablation study and analysis

(1) Study on region-level instance projection

We validate the region-level instance projection (RLIP) strategy proposed for the feature fusion performed in D , and compare it with a regular projection, named Projection. This regular strategy directly projects a conditional vector on the global feature of WSI, which skips a smooth transition from patch to region and region to WSI used in RLIP. Note that the Projection, which makes the fusion of WSI and survival time, is not a scheme appeared in previous literature; it is just used as a WSI-level baseline for comparisons.

From the results of Table 7, we can summarize that (1) RLIP almost always gains C-Index rises (the highest one is +5.36%) on three datasets; (2) at most cases RLIP could decrease MAEs by large degrees (2.61% – 9.93%), and only in a few cases, the MAEs of RLIP increase by no larger than 2.13%; (3) when setting \mathcal{N} to 1-1, RLIP strategy can completely surpass Projection on both C-Index and MAE. These empirical results demonstrate the effectiveness of our region-level strategy. They also suggest that an early feature fusion, *i.e.*, region-level projection rather than a direct WSI-level projection, may be more likely to better incorporate conditional information and help adversarial multiple instance learning.

(2) Study on noise types

We further test the effect of noise type on model performance. Two widely-used distributions of \mathcal{N} , *i.e.*, Uniform and Gaussian, are tested. From the results shown in Table 8, we could see that Uniform distribution could often achieve better performances. Especially in MAE, Uniform ones always have obvious advantages over Gaussian ones. One possible reason is that when sampling \mathcal{N} from Gaussian distribution, the estimation of time-to-event distribution via implicit sampling would be more concentrated and it thereby would tend to enlarge the bias of predictions.

In addition, as mentioned in Section 4.2, we argue that the noise that is combined together with conditional input for prediction may be a critical factor affecting model performance. Some techniques like adversarial training (Goodfellow et al., 2014b; Goodfellow, 2016) may be a promising means to support this argument. We leave this in the future work, since adversarial training is yet another research topic and it is not the focus of this paper.

4.4. Case study and analysis

We randomly select 3 uncensored patients ($\delta = 0$, with event occurrence) and 3 censored patients ($\delta = 1$, without event occurrence) from the test set of NLST. We show these patients' time-to-event estimations provided by the ESAT with AdvMIL and that without AdvMIL, as well as these patients' last follow-up times, in Figure 10.

From these results, we can see that (1) AdvMIL enables ESAT to provide many time-to-event estimations for one pa-

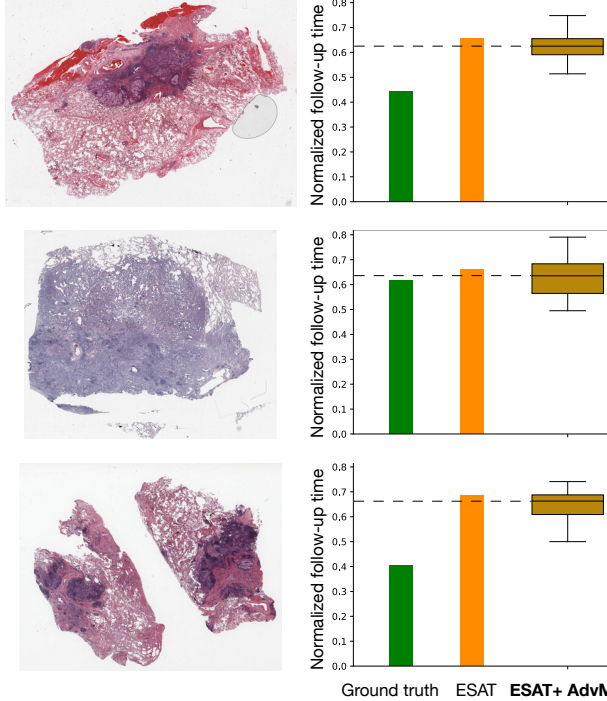
Table 7: Ablation study on region-level instance projection. Δ denotes the improvement of RLIP over regular projection. The MIL encoder of ESAT is adopted.

Noise	Fusion Operation	C-Index \uparrow			MAE \downarrow		
		NLST	BRCA	LGG	NLST	BRCA	LGG
0-1	Projection	0.658 _{0.047}	0.543 _{0.072}	0.624 _{0.084}	0.1983 _{0.0228}	0.0375 _{0.0082}	0.0519 _{0.0064}
	RLIP	0.672 _{0.048}	0.545 _{0.065}	0.621 _{0.063}	0.1871 _{0.0203}	0.0383 _{0.0081}	0.0526 _{0.0058}
	Δ	+ 2.13%	+ 0.37%	- 0.48%	- 5.65%	+ 2.13%	+ 1.35%
1-0	Projection	0.616 _{0.052}	0.548 _{0.084}	0.641 _{0.079}	0.2015 _{0.0243}	0.0344 _{0.0063}	0.0518 _{0.0053}
	RLIP	0.649 _{0.039}	0.562 _{0.067}	0.642 _{0.076}	0.1995 _{0.0240}	0.0349 _{0.0065}	0.0522 _{0.0049}
	Δ	+ 5.36%	+ 2.55%	+ 0.16%	- 9.93%	+ 1.45%	+ 0.77%
1-1	Projection	0.652 _{0.032}	0.531 _{0.080}	0.616 _{0.082}	0.1996 _{0.0213}	0.0389 _{0.0054}	0.0537 _{0.0049}
	RLIP	0.660 _{0.042}	0.545 _{0.075}	0.634 _{0.086}	0.1849 _{0.0153}	0.0366 _{0.0065}	0.0523 _{0.0051}
	Δ	+ 1.23%	+ 2.64%	+ 2.92%	- 7.36%	- 5.91%	- 2.61%

Table 8: Noise effect on AdvMIL performance. The \mathcal{N} with Uniform distribution could often perform better than that with Gaussian distribution. The MIL encoder of ESAT is adopted.

\mathcal{N}	C-Index \uparrow			MAE \downarrow			
	NLST	BRCA	LGG	NLST	BRCA	LGG	
Uniform(0,1)	0-1	0.672 _{0.048}	0.545 _{0.065}	0.621 _{0.063}	0.1871 _{0.0203}	0.0383 _{0.0081}	0.0526 _{0.0058}
	1-0	0.649 _{0.039}	0.562 _{0.067}	0.642 _{0.076}	0.1995 _{0.0240}	0.0349 _{0.0065}	0.0522 _{0.0049}
	1-1	0.660 _{0.042}	0.545 _{0.075}	0.634 _{0.086}	0.1849 _{0.0153}	0.0366 _{0.0065}	0.0523 _{0.0051}
Gaussian(0,1)	0-1	0.632 _{0.039}	0.508 _{0.102}	0.631 _{0.090}	0.1928 _{0.0211}	0.0392 _{0.0063}	0.0567 _{0.0080}
	1-0	0.634 _{0.042}	0.461 _{0.078}	0.624 _{0.050}	0.2011 _{0.0264}	0.0363 _{0.0060}	0.0529 _{0.0033}
	1-1	0.590 _{0.072}	0.554 _{0.047}	0.646 _{0.051}	0.2019 _{0.0223}	0.0403 _{0.0078}	0.0556 _{0.0071}

(a) Survival prediction of **uncensored** patients



(b) Survival prediction of **censored** patients

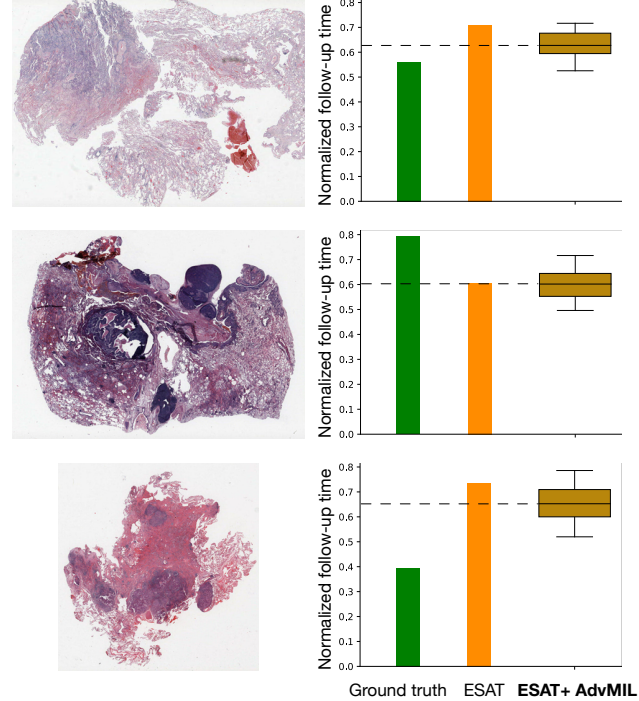


Figure 10: Case study of the time-to-event estimations given by ESAT and its improved version with AdvMIL. Three uncensored patients (left) and three censored patients (right) are randomly selected from the test set of NLST as study samples.

tient while original ESAT gives only one single completely-certain result; (2) the distribution estimation via implicit sampling given by AdvMIL often covers the single point estimation given by ESAT; (3) the median of distribution estimation is often closer to the ground truth than point estimation. However, we cannot quantitatively evaluate the goodness of the distribution coverage given by AdvMIL, because the ground truth of each patient's time-to-event distribution is unknown.

5. Discussion

Gigapixel WSIs contain rich microenvironmental cues that are vital for disease prognosis. An accurate assessment of WSI-based prognosis could help to improve patient management and disease outcomes. Although many end-to-end weakly-supervised models have been developed to estimate patient prognosis from WSIs, their potential is generally restricted by classical survival analysis and fully-supervised learning settings. Inspired by the new idea of adversarial survival modeling, we propose a novel adversarial MIL framework to exploit their potential. This framework could bring new vigor and vitality into the current paradigm of WSI survival analysis by enabling the existing models to estimate a more robust time-to-event distribution and to learn from unlabeled WSI data via semi-supervised training at a relatively low computational cost. We emphasize that this study stands on the shoulders of GANs (Goodfellow et al., 2014a; Mirza and Osindero, 2014) and DATE (Chapfuwa et al., 2018), and shows for the first time how to generalize them to the MIL that is much necessary for WSI representation learning. Last but not least, apart from the technical contributions made by AdvMIL, this study also would like to highlight its practical contribution to computational pathology.

The main limitations of this study include that the goodness of the coverage of distribution estimation cannot be quantitatively evaluated since the ground truth of patient survival distribution is unavailable. In addition, there are also some constraints in our experiments: (1) limited sampling times are adopted to return distribution estimation because it is relatively time-consuming for once-through model inference of a gigapixel image, and (2) our datasets are limited to three cancer types, not covering more datasets and clinical comparisons.

6. Conclusions

This paper proposes a novel framework, adversarial multiple instance learning (AdvMIL), for the survival analysis on gigapixel WSIs. This framework generalizes adversarial time-to-event modeling to the paradigm of MIL mainly by its two important components: the MIL encoder in generator and the fusion network with region-level instance projection in discriminator. It serves as a plug-and-play framework that can be easily and efficiently applied to most end-to-end models of WSI survival analysis. It is demonstrated that the proposed AdvMIL framework could often bring obvious improvements in performance to existing mainstream models at a relatively low computational cost. Most importantly, it could assist these models

to fulfill a more effective estimation of time-to-event distribution and more efficiently learn from unlabeled WSIs in a semi-supervised manner.

References

Carboneau, M.A., Cheplygina, V., Granger, E., Gagnon, G., 2018. Multiple instance learning: A survey of problem characteristics and applications. *Pattern Recognition* 77, 329–353.

Carmon, Y., Raghunathan, A., Schmidt, L., Duchi, J.C., Liang, P.S., 2019. Unlabeled data improves adversarial robustness. *Advances in Neural Information Processing Systems* 32.

Chapelle, O., Scholkopf, B., Zien, Eds., A., 2009. *Semi-Supervised Learning* (Chapelle, O. et al., Eds.; 2006) [Book reviews]. *IEEE Transactions on Neural Networks* 20, 542–542. doi:10.1109/TNN.2009.2015974.

Chapfuwa, P., Tao, C., Li, C., Khan, I., Chandross, K.J., Pencina, M.J., Carin, L., Henao, R., 2020. Calibration and uncertainty in neural time-to-event modeling. *IEEE Transactions on Neural Networks and Learning Systems*.

Chapfuwa, P., Tao, C., Li, C., Page, C., Goldstein, B., Duke, L.C., Henao, R., 2018. Adversarial time-to-event modeling, in: *International Conference on Machine Learning*, PMLR. pp. 735–744.

Chen, R.J., Chen, C., Li, Y., Chen, T.Y., Trister, A.D., Krishnan, R.G., Mahmood, F., 2022a. Scaling vision transformers to gigapixel images via hierarchical self-supervised learning, in: *Proceedings of the IEEE/CVF Conference on Computer Vision and Pattern Recognition*, pp. 16144–16155.

Chen, R.J., Lu, M.Y., Shaban, M., Chen, C., Chen, T.Y., Williamson, D.F., Mahmood, F., 2021. Whole slide images are 2d point clouds: Context-aware survival prediction using patch-based graph convolutional networks, in: *International Conference on Medical Image Computing and Computer-Assisted Intervention*, Springer. pp. 339–349.

Chen, R.J., Lu, M.Y., Williamson, D.F.K., Chen, T.Y., Lipkova, J., Noor, Z., Shaban, M., Shady, M., Williams, M., Joo, B., Mahmood, F., 2022b. Pan-cancer integrative histology-genomic analysis via multimodal deep learning. *Cancer Cell* 40, 865–878.e6. doi:10.1016/j.ccr.2022.07.004.

Cox, D.R., 1975. Partial likelihood. *Biometrika* 62, 269–276.

Deng, J., Dong, W., Socher, R., Li, L.J., Kai Li, Li Fei-Fei, 2009. ImageNet: A large-scale hierarchical image database, in: *2009 IEEE Conference on Computer Vision and Pattern Recognition*, IEEE. pp. 248–255. doi:10.1109/CVPR.2009.5206848.

Dosovitskiy, A., Beyer, L., Kolesnikov, A., Weissenborn, D., Zhai, X., Unterthiner, T., Dehghani, M., Minderer, M., Heigold, G., Gelly, S., et al., 2020. An image is worth 16x16 words: Transformers for image recognition at scale, in: *International Conference on Learning Representations*.

Ghaffari Laleh, N., Muti, H.S., Loeffler, C.M.L., Echle, A., Saldanha, O.L., Mahmood, F., Lu, M.Y., Trautwein, C., Langer, R., Dislich, B., Buelow, R.D., Grabsch, H.I., Brenner, H., Chang-Claude, J., Alwers, E., Brinker, T.J., Khader, F., Truhn, D., Gaisa, N.T., Boor, P., Hoffmeister, M., Schulz, V., Kather, J.N., 2022. Benchmarking weakly-supervised deep learning pipelines for whole slide classification in computational pathology. *Medical Image Analysis* 79, 102474. doi:10.1016/j.media.2022.102474.

Goodfellow, I., 2016. Nips 2016 tutorial: Generative adversarial networks. *arXiv preprint arXiv:1701.00160*.

Goodfellow, I., Pouget-Abadie, J., Mirza, M., Xu, B., Warde-Farley, D., Ozair, S., Courville, A., Bengio, Y., 2014a. Generative adversarial nets. *Advances in neural information processing systems* 27.

Goodfellow, I.J., Shlens, J., Szegedy, C., 2014b. Explaining and harnessing adversarial examples. *arXiv preprint arXiv:1412.6572*.

Gui, J., Sun, Z., Wen, Y., Tao, D., Ye, J., 2021. A review on generative adversarial networks: Algorithms, theory, and applications. *IEEE Transactions on Knowledge and Data Engineering*, 1–1doi:10.1109/TKDE.2021.3130191.

Harrell Jr., F.E., Lee, K.L., Califf, R.M., Pryor, D.B., Rosati, R.A., 1984. Regression modelling strategies for improved prognostic prediction. *Statistics in Medicine* 3, 143–152. doi:<https://doi.org/10.1002/sim.4780030207>.

He, K., Zhang, X., Ren, S., Sun, J., 2016. Deep Residual Learning for Image Recognition, in: *2016 IEEE Conference on Computer Vision and Pattern Recognition (CVPR)*, IEEE. pp. 770–778. doi:10.1109/CVPR.2016.90.

Huang, Z., Chai, H., Wang, R., Wang, H., Yang, Y., Wu, H., 2021. Integration of patch features through self-supervised learning and transformer for survival

analysis on whole slide images, in: International Conference on Medical Image Computing and Computer-Assisted Intervention, Springer. pp. 561–570.

Ilse, M., Tomczak, J., Welling, M., 2018. Attention-based deep multiple instance learning, in: International conference on machine learning, PMLR. pp. 2127–2136.

Kalbfleisch, J.D., Prentice, R.L., 2011. The statistical analysis of failure time data. John Wiley & Sons.

Kallenberg, O., 2002. Foundations of Modern Probability. Springer Science & Business Media.

Kandoth, C., McLellan, M.D., Vandin, F., Ye, K., Niu, B., Lu, C., Xie, M., Zhang, Q., McMichael, J.F., Wyczalkowski, M.A., Leiserson, M.D.M., Miller, C.A., Welch, J.S., Walter, M.J., Wendt, M.C., Ley, T.J., Wilson, R.K., Raphael, B.J., Ding, L., 2013. Mutational landscape and significance across 12 major cancer types. *Nature* 502, 333–339.

Kather, J.N., Krisam, J., Charoentong, P., Luedde, T., Herpel, E., Weis, C.A., Gaiser, T., Marx, A., Valous, N.A., Ferber, D., Jansen, L., Reyes-Aldasoro, C.C., Zörnig, I., Jäger, D., Brenner, H., Chang-Claude, J., Hoffmeister, M., Halama, N., 2019. Predicting survival from colorectal cancer histology slides using deep learning: A retrospective multicenter study. *PLOS Medicine* 16, e1002730. doi:10.1371/journal.pmed.1002730.

Kendall, A., Gal, Y., 2017. What uncertainties do we need in bayesian deep learning for computer vision? *Advances in neural information processing systems* 30.

Kipf, T.N., Welling, M., 2016. Semi-supervised classification with graph convolutional networks. arXiv preprint arXiv:1609.02907.

Lakshminarayanan, B., Pritzel, A., Blundell, C., 2017. Simple and scalable predictive uncertainty estimation using deep ensembles. *Advances in neural information processing systems* 30.

Li, C., Xu, K., Zhu, J., Liu, J., Zhang, B., 2021. Triple generative adversarial networks. *IEEE Transactions on Pattern Analysis and Machine Intelligence*.

Li, R., Yao, J., Zhu, X., Li, Y., Huang, J., 2018. Graph cnn for survival analysis on whole slide pathological images, in: International Conference on Medical Image Computing and Computer-Assisted Intervention, Springer. pp. 174–182.

Linnmans, J., Elfwing, S., van der Laak, J., Litjens, G., 2023. Predictive uncertainty estimation for out-of-distribution detection in digital pathology. *Medical Image Analysis* 83, 102655. doi:10.1016/j.media.2022.102655.

Liu, P., Fu, B., Yang, S.X., Deng, L., Zhong, X., Zheng, H., 2021. Optimizing survival analysis of xgboost for ties to predict disease progression of breast cancer. *IEEE Transactions on Biomedical Engineering* 68, 148–160. doi:10.1109/TBME.2020.2993278.

Liu, P., Fu, B., Ye, F., Yang, R., Xu, B., Ji, L., 2022. Dual-stream transformer with cross-attention on whole-slide image pyramids for cancer prognosis. arXiv preprint arXiv:2206.05782.

Lu, M.Y., Williamson, D.F., Chen, T.Y., Chen, R.J., Barbieri, M., Mahmood, F., 2021. Data-efficient and weakly supervised computational pathology on whole-slide images. *Nature biomedical engineering* 5, 555–570.

Marini, N., Otálora, S., Müller, H., Atzori, M., 2021. Semi-supervised training of deep convolutional neural networks with heterogeneous data and few local annotations: An experiment on prostate histopathology image classification. *Medical Image Analysis* 73, 102165. doi:10.1016/j.media.2021.102165.

Mirza, M., Osindero, S., 2014. Conditional generative adversarial nets. arXiv preprint arXiv:1411.1784.

Miyato, T., Koyama, M., 2018. cgans with projection discriminator, in: International Conference on Learning Representations.

Miyato, T., Maeda, S.i., Koyama, M., Ishii, S., 2018. Virtual adversarial training: a regularization method for supervised and semi-supervised learning. *IEEE transactions on pattern analysis and machine intelligence* 41, 1979–1993.

Nazarovs, J., Huang, Z., Tasneeyapant, S., Chakraborty, R., Singh, V., 2022. Understanding uncertainty maps in vision with statistical testing, in: Proceedings of the IEEE/CVF Conference on Computer Vision and Pattern Recognition, pp. 406–416.

Nir, G., Hor, S., Karimi, D., Fazli, L., Skinnider, B.F., Tavassoli, P., Turbin, D., Villamil, C.F., Wang, G., Wilson, R.S., Iczkowski, K.A., Lucia, M.S., Black, P.C., Abolmaesumi, P., Goldenberg, S.L., Salcudean, S.E., 2018. Automatic grading of prostate cancer in digitized histopathology images: Learning from multiple experts. *Medical Image Analysis* 50, 167–180.

doi:10.1016/j.media.2018.09.005.

Salimans, T., Goodfellow, I., Zaremba, W., Cheung, V., Radford, A., Chen, X., 2016. Improved techniques for training gans. *Advances in neural information processing systems* 29.

Shao, W., Wang, T., Huang, Z., Han, Z., Zhang, J., Huang, K., 2021. Weakly supervised deep ordinal cox model for survival prediction from whole-slide pathological images. *IEEE Transactions on Medical Imaging* 40, 3739–3747.

Shen, Y., Liu, L., Tang, Z., Chen, Z., Ma, G., Dong, J., Zhang, X., Yang, L., Zheng, Q., 2022. Explainable survival analysis with convolution-involved vision transformer, in: Proceedings of the AAAI Conference on Artificial Intelligence, AAAI Press. pp. 2207–2215.

Skrede, O.J., De Raedt, S., Kleppe, A., Hveem, T.S., Liestøl, K., Maddison, J., Askautrud, H.A., Pradhan, M., Nesheim, J.A., Albrechtsen, F., Farstad, I.N., Domingo, E., Church, D.N., Nesbakken, A., Shepherd, N.A., Tomlinson, I., Kerr, R., Novelli, M., Kerr, D.J., Danielsen, H.E., 2020. Deep learning for prediction of colorectal cancer outcome: a discovery and validation study. *The Lancet* 395, 350–360. doi:10.1016/S0140-6736(19)32998-8.

Springenberg, J.T., 2015. Unsupervised and semi-supervised learning with categorical generative adversarial networks. arXiv preprint arXiv:1511.06390.

Team, N.L.S.T.R., 2011. The national lung screening trial: overview and study design. *Radiology* 258, 243–53. doi:<https://doi.org/10.1148/radiol.10091808>.

Uemura, T., Näppi, J.J., Watari, C., Hironaka, T., Kamiya, T., Yoshida, H., 2021. Weakly unsupervised conditional generative adversarial network for image-based prognostic prediction for covid-19 patients based on chest ct. *Medical Image Analysis* 73, 102159.

Wei, L.J., 1992. The accelerated failure time model: A useful alternative to the cox regression model in survival analysis. *Statistics in Medicine* 11, 1871–1879. doi:10.1002/sim.4780111409.

Wulczyn, E., Steiner, D.F., Moran, M., Plass, M., Reihls, R., Tan, F., Flament-Auvigne, I., Brown, T., Regitnig, P., Chen, P.H.C., Hegde, N., Sadhwani, A., MacDonald, R., Ayalew, B., Corrado, G.S., Peng, L.H., Tse, D., Müller, H., Xu, Z., Liu, Y., Stumpe, M.C., Zatloukal, K., Mermel, C.H., 2021. Interpretable survival prediction for colorectal cancer using deep learning. *npj Digital Medicine* 4, 71. doi:10.1038/s41746-021-00427-2.

Yao, J., Zhu, X., Jonnagaddala, J., Hawkins, N., Huang, J., 2020. Whole slide images based cancer survival prediction using attention guided deep multiple instance learning networks. *Medical Image Analysis* 65, 101789.

Yu, K.H., Zhang, C., Berry, G.J., Altman, R.B., Ré, C., Rubin, D.L., Snyder, M., 2016. Predicting non-small cell lung cancer prognosis by fully automated microscopic pathology image features. *Nature Communications* 7, 12474. doi:10.1038/ncomms12474.

Zadeh, S.G., Schmid, M., 2021. Bias in cross-entropy-based training of deep survival networks. *IEEE Transactions on Pattern Analysis and Machine Intelligence* 43, 3126–3137. doi:10.1109/TPAMI.2020.2979450.

Zarella, M.D., Bowman, D., Aeffner, F., Farahani, N., Xthona, A., Absar, S.F., Parwani, A., Bui, M., Hartman, D.J., 2018. A Practical Guide to Whole Slide Imaging: A White Paper From the Digital Pathology Association. *Archives of Pathology & Laboratory Medicine* 143, 222–234. doi:10.5858/arpa.2018-0343-RA.

Zhou, X., Jiao, Y., Liu, J., Huang, J., 2022. A deep generative approach to conditional sampling. *Journal of the American Statistical Association*, 1–12.

Zhou, Z.H., 2021. Semi-Supervised Learning, in: Machine Learning. Springer Singapore, Singapore, pp. 315–341. doi:10.1007/978-981-15-1967-3\13.